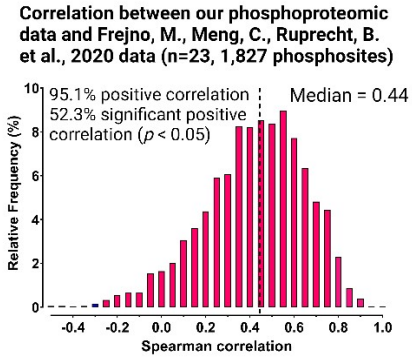

Supplemental Figure 1. Comparison between our phosphoproteomics data and data from a previously reported large-scale phosphoproteomics study of CRC cell lines, related to Figure 1.

Spearman's correlation between our phosphoproteomics data and data from Frejno, M., Meng, C., Ruprecht B, et al. (2020). The 1,827 phosphosites across 23 CRC cell lines shared in both datasets were used in this study.

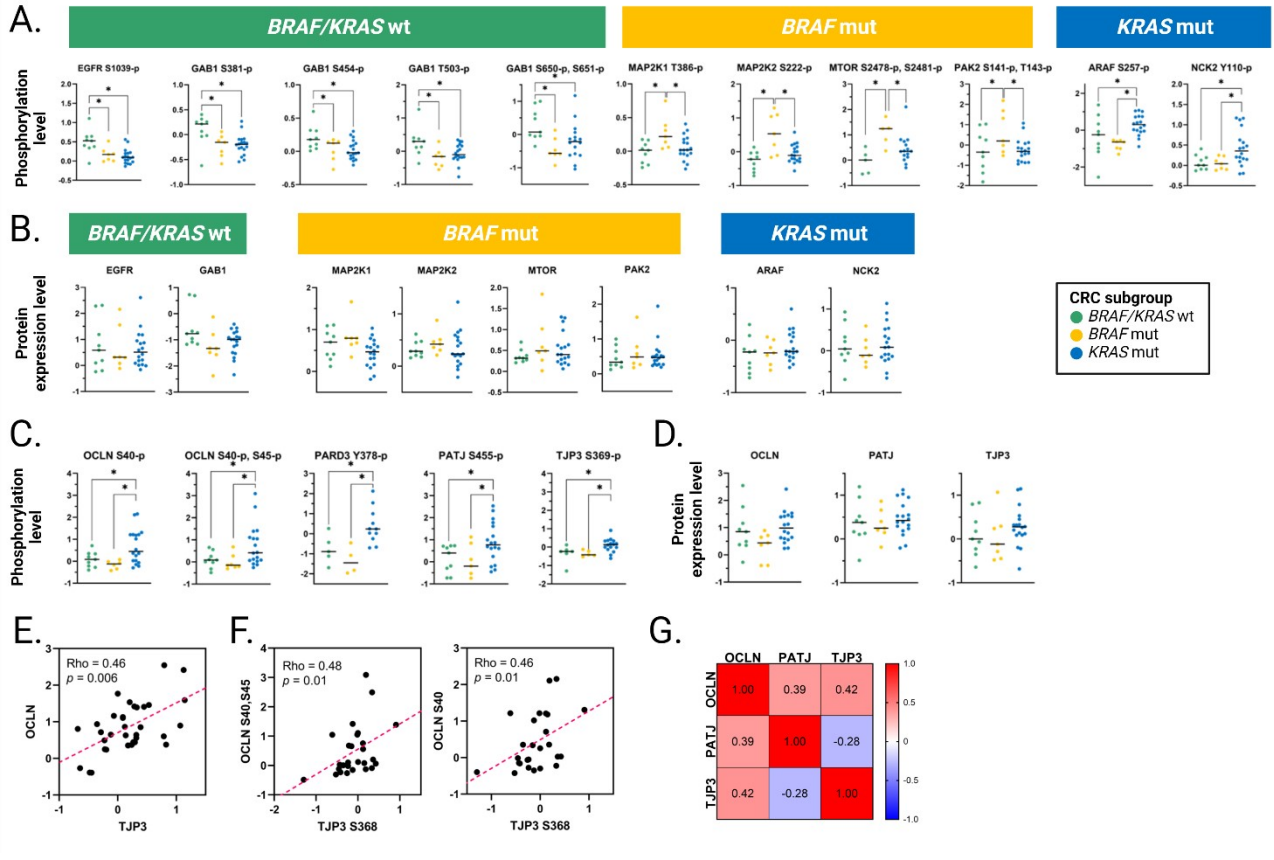

Supplemental Figure 2. Boxplots and correlation matrix of proteins and phosphorylation sites in the enriched pathway that showed differential expression between the CRC subgroups, related to Figure 2.

A. Beeswarm plots of the 11 phosphosites of the ErbB signalling pathway showing differential regulation among CRC subgroups. The horizontal line represents the median.

B. Beeswarm plots of the 8 proteins of the ErbB signalling pathway among CRC subgroups. The horizontal line represents the median.

C. Beeswarm plots of the 5 phosphorylation sites of tight junction signalling showing differential regulation among CRC subgroups. The horizontal line represents the median.

D. Beeswarm plots of the 3 protein components of tight junction signalling among CRC subgroups. The horizontal line represents the median.

E. Correlation plot of the protein expression levels of TJP3 and OCLM.

F. Correlation plot of the phosphorylation levels of TJP3 S368 and OCLM S40 and S45.

G. Correlation matrix of the proteome expression levels of the key components of tight junctions in KRAS-mut cell lines (Spearman's test).

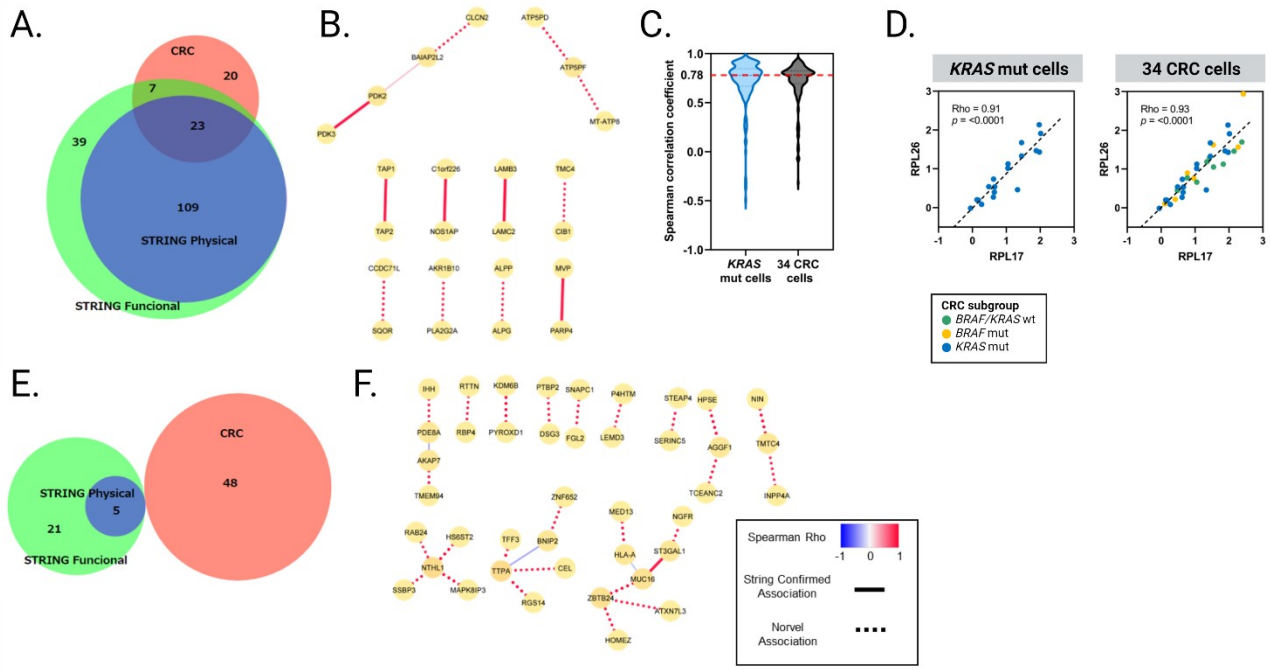

Supplemental Figure 3. Protein coregulation analysis for the identification of protein–protein associations in KRAS-mutant cells, related to Figure 3.

A. Venn diagram of the commonly occurring protein pairs (the bottom 10% of protein–protein interactions of the correlation difference) among STRING physical dataset, STING functional dataset and our CRC dataset.

B. Protein–protein association network of the commonly occurring protein pairs (bottom 10%), related to Fig. 3B.

C. Violin plot of the Spearman's correlation coefficient of functional protein–protein associations based on the STRING database between KRAS-mutant cells and 34 CRC cell types.

D. Correlation plot of the protein expression levels of RPL17 and RPL26 in KRAS-mutant cells and 34 other CRC cell lines.

E. Venn diagram of the KRAS-specific protein pairs (the top 10% of protein–protein interactions

of the correlation difference) among the STRING physical dataset, STING functional dataset and our CRC dataset.

F. Protein–protein association network of KRAS-specific protein pairs (top 10%) of the correlation difference, related to Fig. 3D.

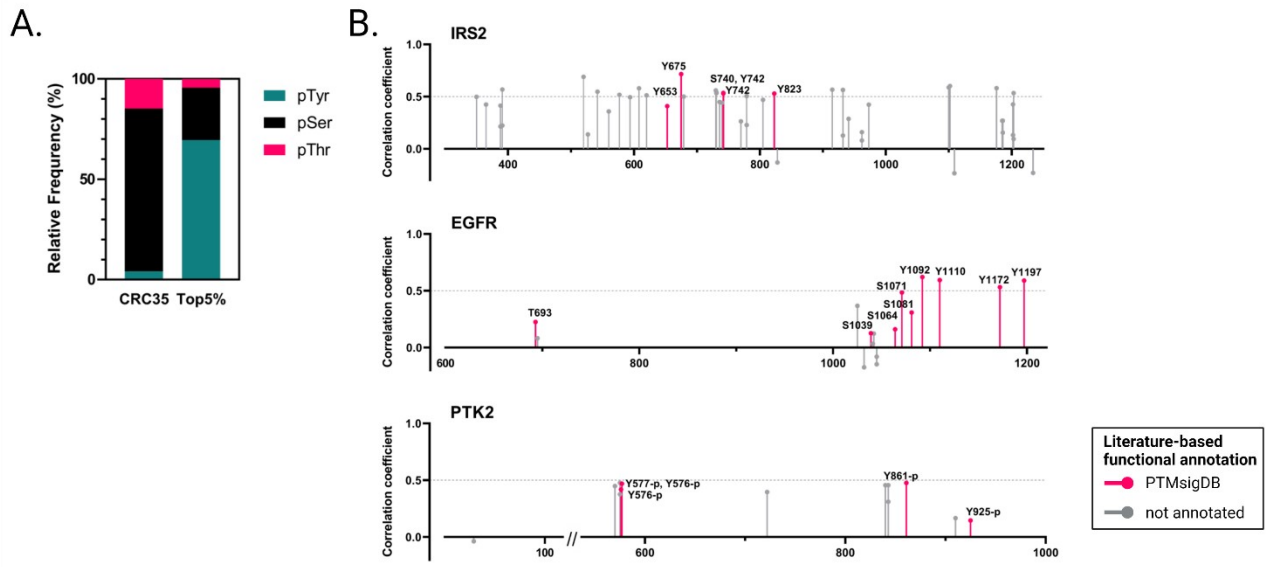

Supplemental Figure 4. Features of phosphorylation sites showing a high correlation between phosphorylation levels and gene dependency scores, related to Figure 4.

A. Distribution comparing the relative frequency of phosphoserine (pSer, black), phosphothreonine (pThr, red), and phosphotyrosine (pTyr, green) in the top 5% highly correlated phosphosites with gene dependency scores with that in all quantified phosphosites in CRC35.

B. Spearman's correlation coefficient of phosphorylation sites identified in IRS2 (top), EGFR (middle) and PTK2 (down) with unknown (grey) and known activation in PTMsigDB (deep pink).

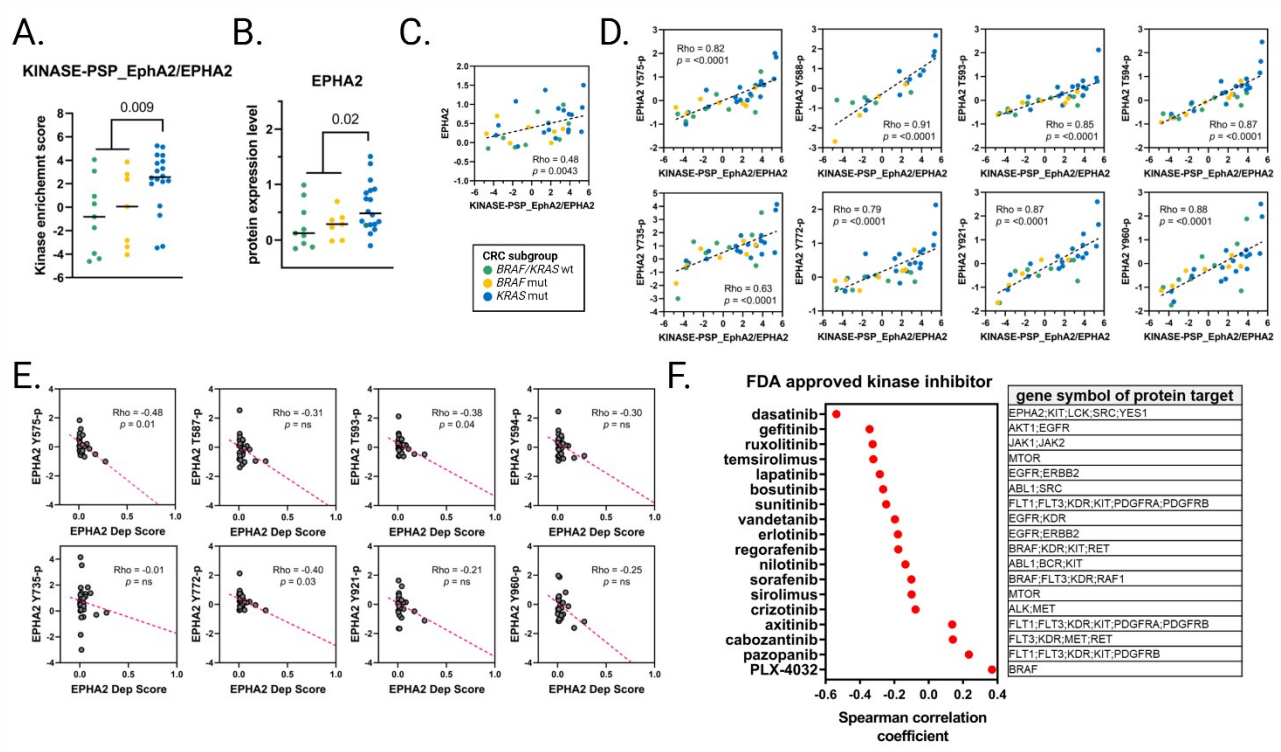

Supplemental Figure 5. Potential therapeutic opportunity for KRAS-mutant cells, related to Figure 5.

A. Beeswarm plots of EPHA2 kinase enrichment scores showing differential enrichment between the CRC subgroups (p value = 0.009, Welch's t test between KRAS mut vs. (BRAF mut and BRAF/KRAS wt)).

B. Beeswarm plots of EPHA2 protein expression levels showing differential expression between the CRC subgroups (p value = 0.02, Welch's t test between KRAS mut vs. BRAF mut and BRAF/KRAS wt).

C. Correlation plots between EPHA2 kinase enrichment scores and protein expression levels of EPHA2.

D. Correlation plots between EPHA2 kinase enrichment scores and phosphorylation levels of substrates on EPHA2.

E. Correlation plots between EPHA2 dependency scores and phosphorylation levels of substrates on EPHA2.

F. List of Spearman's correlation coefficients between phosphorylation levels of PARD3 Y378 and CTD2 AUCs of FDA-approved kinase inhibitors. Gene symbols of the protein targets for each inhibitor are shown in the right table.

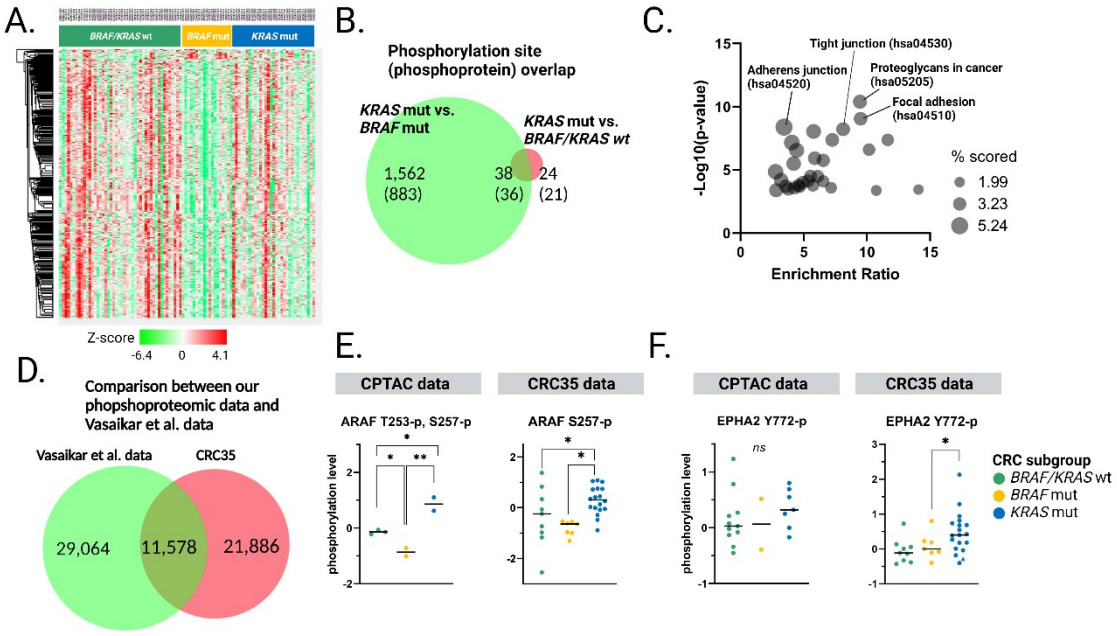

Supplemental Figure 6. Comparison of the phosphoproteomic data of CRC35 with data from the CPTAC Colon Cancer Study

A. Hierarchical clustering of 4,103 significantly regulated phosphorylation sites according to the KRAS and BRAF mutational status (p value < 0.05, FDR < 0.1, one-way ANOVA followed by Tukey's post hoc test).

B. Venn diagram of significantly upregulated phosphorylation sites (phosphoproteins) in the KRAS mut vs. BRAF mut or KRAS mut vs. BRAF/KRAS wt subgroups.

C. Bubble plot of the KEGG pathway enrichment of differentially expressed genes (DEGs) in the KRAS mut group. The bubble size corresponds to the % scored in the pathway. The % score indicates the ratio of the number of DEGs mapped to a certain pathway to the total number of genes mapped to the pathway.

D. Venn diagram demonstrating the overlap between in-house CRC35 phosphoproteomic data and CPTAC phosphoproteomic data (Vasaikar, et al. 2019).

E. and F. Beeswarm plots of the phosphorylation levels of ARAF-T253, S257 (E), and EPHA2-Y772 (F) showing differential regulation among the various KRAS and BRAF mutational status subgroups in the CPTAC data (left) and CRC35 data (right). The horizontal line represents the median.